Internal Wave Reflection on Shelf Slopes with Depth-Varying Stratification

ROB A. HALL

School of Environmental Sciences, University of East Anglia, Norwich, United Kingdom

JOHN M. HUTHNANCE

National Oceanography Centre, Liverpool, United Kingdom

RICHARD G. WILLIAMS

School of Environmental Sciences, University of Liverpool, Liverpool, United Kingdom

(Manuscript received 21 October 2011, in final form 15 October 2012)

ABSTRACT

Reflection of internal waves from sloping topography is simple to predict for uniform stratification and linear slope gradients. However, depth-varying stratification presents the complication that regions of the slope may be subcritical and other regions supercritical. Here, a numerical model is used to simulate a mode-1, M_2 internal tide approaching a shelf slope with both uniform and depth-varying stratifications. The fractions of incident internal wave energy reflected back offshore and transmitted onto the shelf are diagnosed by calculating the energy flux at the base of slope (with and without topography) and at the shelf break. For the stratifications/topographies considered in this study, the fraction of energy reflected for a given slope criticality is similar for both uniform and depth-varying stratifications. This suggests the fraction reflected is dependent only on maximum slope criticality and independent of the depth of the pycnocline. The majority of the reflected energy flux is in mode 1, with only minor contributions from higher modes due to topographic scattering. The fraction of energy transmitted is dependent on the depth-structure of the stratification and cannot be predicted from maximum slope criticality. If near-surface stratification is weak, transmitted internal waves may not reach the shelf break because of decreased horizontal wavelength and group velocity.

1. Introduction

Internal waves play an important role in supporting mixing on continental shelf slopes through critical reflection and breakdown into turbulence (Wunsch 1968; Eriksen 1982; Gilbert and Garrett 1989). They are generated by atmospheric forcing or across-slope tidal flow and may propagate long distances (Alford et al. 2007) before reflecting from remote topography (Nash et al. 2004).

Behavior of normally incident internal waves approaching a shelf slope from offshore can be predicted from α, the ratio of the topographic slope to the internal wave characteristic slope,

$$\alpha = \frac{s_{\text{topog}}}{s_{\text{wave}}} = \frac{\partial H/\partial x}{[(\omega^2 - f^2)/(N^2 - \omega^2)]^{1/2}}, \tag{1}$$

where H is the total depth, x across-slope distance, ω the angular frequency of the wave, f the inertial frequency, and N the buoyancy frequency. If $\alpha < 1$ (subcritical) waves will be transmitted onto the shelf. If $\alpha > 1$ (supercritical) waves will be partially reflected back offshore. If $\alpha = 1$ (critical) linear theory breaks down, leading to nonlinear effects, wave breaking, and turbulent mixing (Ivey and Nokes 1989; Dauxois et al. 2004). For obliquely incident internal waves, the effective slope has a different criticality (Eriksen 1982; Martini et al. 2011).

For flat bottom cases, internal wave motions can be decomposed into vertical normal modes, determined by the buoyancy frequency profile. Mode-1 waves have a single zero crossing for horizontal velocity (e.g., Fig. 1a) and high phase speed. They are scattered to higher

Corresponding author address: Rob A. Hall, School of Environmental Sciences, University of East Anglia, Norwich Research Park, Norwich, NR4 7TJ, United Kingdom.
E-mail: robert.hall@uea.ac.uk

DOI: 10.1175/JPO-D-11-0192.1

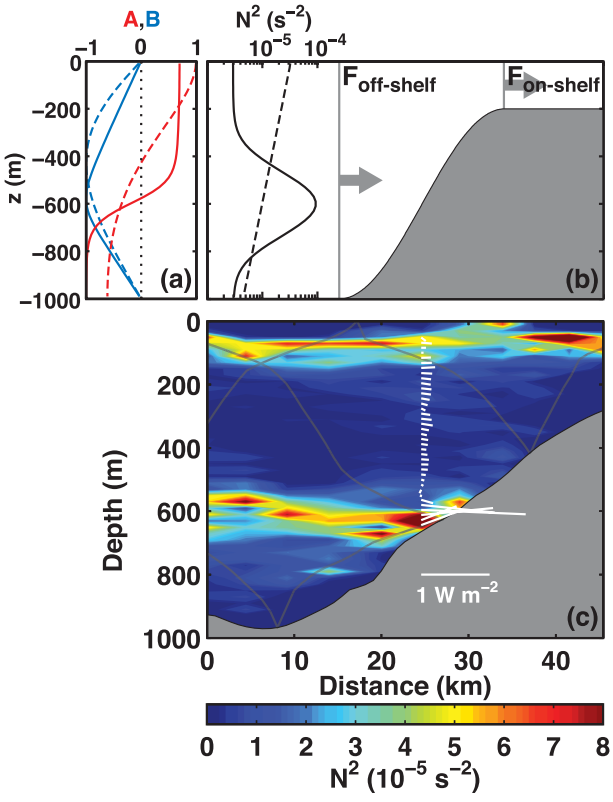

FIG. 1. (a) Mode-1 profiles of horizontal (red lines) and vertical (blue lines) velocity for near-surface (dashed lines) and middepth (solid lines) stratification. (b) An example of model topography showing "off-shelf" and "on-shelf" locations and N^2 for near-surface and middepth stratification. (c) Vectors of M_2 internal tide energy flux on the West Shetland slope and the across-slope N^2 field. The gray lines are M_2 internal tide characteristics.

modes (multiple zero-crossings and lower phase speed) by reflection from topography (Johnston and Merrifield 2003), the superposition of which results in the formation of internal wave beams (Lamb 2004; Akylas et al. 2007; Cole et al. 2009; Mathur and Peacock 2009). These beams have the same gradient as the internal wave characteristic (s_{wave}).

This study is prompted by observations of an internal tide on the West Shetland slope, the shelf slope north of Scotland (Hall et al. 2011). Over the slope there is a strong middepth pycnocline that separates two low-buoyancy water masses. The internal tide is primarily semidiurnal and the M_2 energy flux is concentrated in the pycnocline (Fig. 1c). The shelf slope is supercritical to the internal tide where it is intersected by the pycnocline, but subcritical above and below. These observations raise the question of how internal waves behave on slopes that are both sub- and supercritical.

Most investigations of internal wave breaking on slopes using tank experiments (e.g., Cacchione and Wunsch 1974; Ivey and Nokes 1989; De Silva et al. 1997; Dauxois et al. 2004) and numerical models (e.g., Slinn and Riley 1996; Legg and Adcroft 2003) have considered uniform stratification cases. However, the real ocean is rarely uniformly stratified. Nash et al. (2004) investigated low-mode, semidiurnal internal tide reflection on a nonuniformly stratified continental slope and observed scattering to higher vertical wavenumbers and elevated near-bottom mixing. Klymak et al. (2011) observed supercritical reflection of the diurnal internal tide on a continental slope and, using a linear scattering model, noted that the fractions of energy transmitted and reflected are sensitive to the phase between the modal components of the incident wave.

Here, numerical model simulations of internal waves approaching a shelf slope are conducted to assess how much internal wave energy is reflected and transmitted if α varies spatially due to a combination of depth-varying stratification and curved slope topography.

2. Numerical model setup

We consider the case of a mode-1, M_2 internal tide approaching a shelf slope from a remote, deep water source. Internal wave generation on the slope itself (e.g., Baines 1982; Maas 2011) is not considered. The Massachusetts Institute of Technology General Circulation Model (MITgcm, Marshall et al. 1997) is used following the work of Legg and Adcroft (2003) on internal wave breaking on concave and convex continental slopes. Here, stratification and slope topography are varied, both of which affect the value of α.

The model is run in nonhydrostatic mode, with a linear free surface condition, but without rotation ($f = 0$). It is configured in two-dimensions (across-slope and vertical); the left-hand side of the domain is 1000 m deep with a flat bottom, in the middle of the domain there is the shelf slope, and on the right-hand side a 200 m deep continental shelf (Fig. 1b). A linear equation of state is used. Viscosity and horizontal diffusivity are uniform ($\nu_h = 10^{-2}$ m^2 s^{-1}, $\nu_z = 10^{-3}$ m^2 s^{-1}, and $\kappa_h = 10$ m^2 s^{-1}); vertical diffusivity is calculated implicitly.

Initial conditions are no-flow and horizontally uniform stratification. Three initial stratification profiles are considered: uniform stratification (UniStrat, $N^2 = 0.3 \times 10^{-5}$ s^{-2}), near-surface stratification (SurfStrat) modeled on observed potential temperature profiles from the shelf slope off California, and middepth stratification (MidStrat) modeled on profiles from the the base of West Shetland slope (Fig. 1b). Depth-averaged N^2 is the same for both depth-varying stratification cases (1.3×10^{-5} s^{-2}). Salinity is uniform.

TABLE 1. Range of N^2, off-shelf and on-shelf mode-1 horizontal phase velocity (c_p), internal wave characteristic slope (s_{wave}), topographic slope (s_{topog}), and nondimensional parameters for each model run. For the UniStrat case, α is uniform; for the SurfStrat and MidStrat cases, $\alpha_{\max}$ is shown. Fr_I and Fr_R are the incident and reflected wave Froude numbers respectively. l_{eff} is the effective slope width and h_{eff} the effective slope height. The runs shown in Figs. 3 and 4 are in bold.

		c_p (m s^{-1})								
Stratification	N^2 (s^{-2})	off-shelf	on-shelf	Fr_I	s_{wave}	s_{topog}	$\alpha_{(\max)}$	$\text{Fr}_{R(\max)}$	l_{eff}	h_{eff}
UniStrat	0.3×10^{-5}	0.55	0.11	0.05	0.08	0.02	0.25	0.1	2.71	0.8
						0.04	0.5	0.4	1.36	0.8
						0.06	0.75	2.0	0.90	0.8
						0.08	1.0	$\gg 1$	0.68	0.8
						0.12	1.5	1.2	0.47	0.8
						0.16	2.0	0.4	0.34	0.8
						0.2	2.5	0.3	0.27	0.8
SurfStrat	$0.5–3.2 \times 10^{-5}$	1.18	0.33	0.02	0.02–007	$\leq$0.01	0.2	0.1	3.54	0.7
						$\leq$0.02	**0.5**	**0.2**	**1.77**	**0.7**
						$\leq$0.03	0.7	0.9	1.19	0.7
						$\leq$0.04	1.0	$\gg 1$	0.89	0.7
						$\leq$0.05	**1.2**	**$\gg 1$**	**0.72**	**0.7**
						$\leq$0.075	1.8	$\gg 1$	0.48	0.7
						$\leq$0.1	2.4	$\gg 1$	0.35	0.7
MidStrat	$0.3–9.3 \times 10^{-5}$	1.93	0.11	0.01	0.01–0.08	$\leq$0.005	0.3	0.1	6.37	0.9
						$\leq$0.01	**0.7**	**0.4**	**3.19**	**0.9**
						$\leq$0.015	1.0	$\gg 1$	2.12	0.9
						$\leq$0.02	**1.4**	**$\gg 1$**	**1.59**	**0.9**
						$\leq$0.03	2.1	$\gg 1$	1.07	0.9
						$\leq$0.04	2.8	$\gg 1$	0.80	0.9
						$\leq$0.05	3.5	$\gg 1$	0.64	0.9

Boundary conditions are no-slip at the bottom, no-stress at the surface, and no buoyancy flux at either. Oscillating velocities and temperature anomalies, consistent with a mode-1, M_2 internal tide propagating toward the slope, are prescribed at the off-shelf boundary,

$$u(0,z,t) = U_0 A(z)\sin(\omega t), \tag{2}$$

$$w(0,z,t) = U_0\left[\frac{\omega^2}{N^2(z)-\omega^2}\right]^{1/2} B(z)\cos(\omega t), \quad \text{and} \tag{3}$$

$$\theta(0,z,t) = \theta_0(z) - U_0\frac{N(z)}{gC_\theta}B(z)\sin(\omega t), \tag{4}$$

where $U_0 = 2.5$ cm s^{-1} is the forcing amplitude, $\omega = 1.4 \times 10^{-4}$ s^{-1} the frequency, $\theta_0(z)$ the initial potential temperature profile, and C_θ the thermal expansion coefficient. $A(z)$ and $B(z)$ are mode-1 profiles of horizontal and vertical velocity, respectively (Fig. 1a). For the uniform stratification case, $A(z) = \cos(\pi z/H_0)$ and $B(z) = \sin(\pi z/H_0)$, where H_0 is the total depth at the off-shelf boundary. The forcing is ramped up over two tidal cycles to avoid transients.

The gradient of the shelf slope (s_{topog}) is adjusted to change α. For the uniform stratification case, a linear slope is used so that α is uniform across isobaths. For the depth-varying stratification cases, a sinusoidal slope is used so that, combined with $N^2(z)$, α varies between isobaths.

For each stratification case, 7 runs are completed with $\alpha_{\max}$ ranging from less than 0.5 to more than 2 (Table 1). The horizontal and vertical resolutions are 250 and 20 m, respectively, and the length of the domain is adjusted to maintain consistency between runs; the base of the slope is located 4 mode-1 horizontal wavelengths (for a 1000 m watercolumn) from the off-shelf boundary. The total length of the domain is 8 wavelengths.

3. Diagnostics

The model is run for 18 tidal cycles ($18T$). Full-amplitude internal waves reach the base of the shelf slope at $6T$ and interference due to reflection from the offshore boundary occurs after $12T$. Snapshots at $t = 10.25T$ of across-slope velocity (u) and vertical displacement (ξ) of isopycnals (centered on 100-m separated levels) are shown for both near-surface stratification and middepth stratification examples. To aid comparison, horizontal distance is referenced to zero at the base of the slope.

Internal tide energy flux is calculated as $\mathbf{F} = \langle \mathbf{u}'p' \rangle$, where $\mathbf{u}'$ is the velocity perturbation (u', w'), p' the pressure perturbation, and $\langle \cdot \rangle$ denotes an average over a tidal cycle (e.g., Kunze et al. 2002; Nash et al. 2005); The quantity $\mathbf{F}$ is calculated for the cycle $10–11T$. To

separate the net internal tide energy flux at the base of the slope ($\mathbf{F}_{\text{off-shelf}}$) into incident (onshore propagating) and reflected (offshore propagating) components without complex demodulation (Mercier et al. 2008), three control runs without topography are completed, one for each stratification case. The energy flux from the control run is considered the incident wave. The net energy flux from the run with topography contains both the incident and reflected waves so the residual after subtracting the energy flux from the control run is considered the reflected wave (i.e., Net = Incident + Reflected). The transmitted internal tide energy flux is diagnosed at the shelf break ($\mathbf{F}_{\text{on-shelf}}$). For some MidStrat runs, $\mathbf{F}_{\text{on-shelf}}$ is calculated for a later tidal cycle because it takes longer for full-amplitude internal waves to reach the shelf. The difference between net energy flux at the base of the slope and transmitted energy flux ($\mathbf{F}_{\text{off-shelf}} - \mathbf{F}_{\text{on-shelf}}$) is assumed to be numerical dissipation and not discussed further.

Modal decomposition of the internal tide energy flux is accomplished from least squares fits of $\mathbf{u}'$ to vertical normal modes (Dushaw et al. 1995; Nash et al. 2005). The net, incident, and reflected energy fluxes are decomposed at the base of the slope. At the shelf break, only the net energy flux is decomposed.

Several nondimensional parameters are calculated to characterize the internal wave behavior. The topographic–internal wave characteristic slope ratio (α, Eq. 1) is uniform for the uniform stratification case but varies spatially for the depth-varying stratification cases. For the depth-varying stratifications, the maximum α-value ($\alpha_{\max}$) is used as a metric even though it only characterizes a single point on the slope.

Reflected and incident wave Froude numbers are calculated following Phillips (1977) and Legg and Adcroft (2003) to characterize the nonlinearity of the flow. The incident wave Froude number, $\text{Fr}_I = U_0/c_p$, where c_p is the mode-1 horizontal phase velocity at the base of the slope, is small ($\text{Fr}_I < 0.1$) for all stratification cases and the incident internal wave behaves as a linear wave. The reflected wave Froude number,

$$\text{Fr}_R = \text{Fr}_I \left[\frac{\sin(\beta + \gamma)}{\sin(|\beta - \gamma|)} \right]^2, \tag{5}$$

where $\beta = \tan^{-1}(s_{\text{wave}})$ is the angle of the internal wave characteristic to the horizontal and $\gamma = \tan^{-1}(s_{\text{topog}})$ the angle of the topography to the horizontal, varies spatially for depth-varying stratifications and/or curved slope topographies and goes to ∞ at critical slopes. Fr_R (or maximum Fr_R) for each run is shown in Table 1. Nonlinear, internal bore behavior is predicted for $\text{Fr}_R > 1$ so may be expected for all near-critical ($0.75 < \alpha < 1.5$) and partially supercritical (i.e., subsuper–subcritical) slope runs. However, internal bores and other nonhydrostatic process cannot be fully resolved with 250-m horizontal resolution.

The effective width of the slope, relative to the mode-1 horizontal wavelength, is calculated $l_{\text{eff}} = l/\overline{\lambda}$, where l is the actual slope width (base of the slope to the shelf break) and $\overline{\lambda}$ the average mode-1 horizontal wavelength across the slope (Table 1). As the water depth decreases mode-1 horizontal wavelength also decreases, so the average wavelength is dependent on both the buoyancy frequency profile and the slope topography. Effective slope width is typically large for subcritical slopes and small for (partially) supercritical slopes, but, for a given value of $\alpha_{(\max)}$, l_{eff} is more than a factor of 2 larger for the MidStrat case than for either the SurfStrat or UniStrat cases. This is the result of drastically decreased depth-averaged N^2 and horizontal wavelength up-slope of the 600-m isobath (the depth of the pycnocline) in the MidStrat case.

4. Results

a. Uniform stratification

The UniStrat runs demonstrate the transition from subcritical transmission to supercritical reflection for the simple case where α is uniform. Consistent with critical slope theory, the fraction of incident internal wave energy reflected back offshore increases with increasing α; near-zero for subcritical slopes, increasing to over 80% for the most supercritical slope (Fig. 2a). The fraction of energy reflected is dominated by the lowest internal wave mode; the fraction reflected to mode 1 increases with increasing α, while the fraction reflected to higher modes (2 to 5) is roughly constant, ~30%.

Also consistent with critical slope theory, the fraction of energy transmitted onto the shelf initially increases with decreasing α (Fig. 2b). As the mode-1 waves propagate up the slope and onto the shelf, there is an 80% decrease in horizontal phase (and group) velocity (Table 1), the same as the decrease in water depth. For $\alpha < 0.5$, the fraction of energy transmitted decreases with decreasing α because the waves have to propagate further to reach the shelf break and are likely dissipated by multiple surface and bottom reflections. The maximum fraction transmitted is 35%.

b. Near-surface stratification

The SurfStrat runs show the effect of N^2 decreasing with depth combined with curved slope topography. The term $\alpha_{\max}$ occurs at 450 m, near the top of the shelf slope; the base of the slope is always subcritical. The fraction of incident internal wave energy reflected back offshore with respect to $\alpha_{\max}$ closely follows the UniStrat

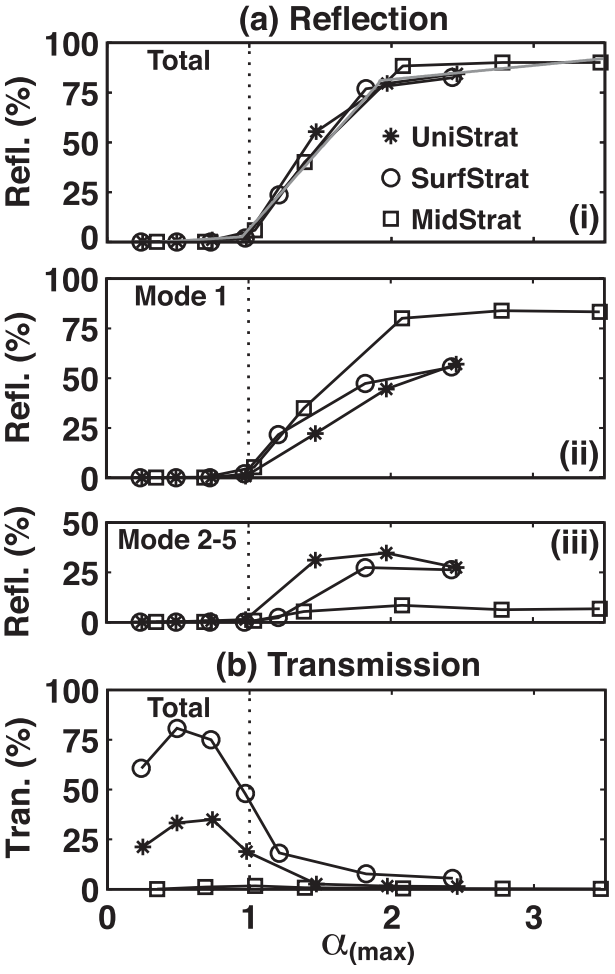

FIG. 2. Fractions of incident internal wave energy (a) reflected back offshore and (b) transmitted onto the shelf for each model run, plotted against $\alpha_{(\max)}$. (i) Total reflected energy, (ii) reflected energy in mode 1, (iii) reflected energy in modes 2 to 5. The gray line in (i) is a piece-wise linear regression for all runs.

case (Fig. 2a) and the majority of the reflected energy is in mode 1. For $\alpha_{\max} > 1.5$, the fraction of energy reflected to higher modes is ~25%. The fraction transmitted onto the shelf is larger than that for the UniStrat case (up to 81%) because only a single point on the slope is characterized by $\alpha_{\max}$ (Fig. 2b) and the decrease in horizontal group velocity as the waves propagate onto the shelf is less (72%).

Looking at a subcritical slope example in more detail (Fig. 3a), the forced mode-1 structure is maintained up onto the shelf, with near-surface and near-bottom energy fluxes amplified at the shelf break as the transmitted waves shoal. For a partially supercritical slope example, where $\alpha > 1$ between 300 and 690 m and $\alpha_{\max} = 1.2$ (Fig. 3b), internal wave beams are apparent, originating in the upper near-critical region close to the shelf break and propagating both onto the shelf and back offshore. The energy flux is bottom intensified on the near- and supercritical upper slope. Modal decomposition of the energy flux at the base of the slope shows only 3% is contained in higher modes; depth-integrated, the higher-mode energy fluxes are all offshore. At the shelf break however, 36% of the energy is contained in higher modes (not shown).

Maximum reflected energy flux is at the surface and bottom (Fig. 5a), consistent with reflection of internal wave characteristics from the supercritical region of the slope. However, modal decomposition shows the majority of the reflected energy flux is in mode 1, with minor contributions from higher modes due to topographic scattering.

c. *Middepth stratification*

The MidStrat runs show what happens if N^2 and the topographic slope are maximum at the same depth. $\alpha_{\max}$ occurs at 600 m, in the middle of the shelf slope; the base and top of the slope are always subcritical. As with the SurfStrat runs, the fraction of incident internal wave energy reflected back offshore closely follows the UniStrat case (Fig. 2a). Again, the majority of the reflected energy is in mode 1, only ~5% is reflected to higher modes.

The fraction of energy transmitted onto the shelf is less than 2% for all MidStrat runs. Even if the slope is entirely subcritical, the transmitted waves are almost entirely dissipated before reaching the shelf break (Fig. 2b). This is an effect of the low near-surface buoyancy frequency (compared to the depth-average), which causes horizontal group velocity to decrease by almost 95% as the waves propagate up the slope and results in a far longer effective slope width than either the UniStrat or SurfStrat cases. The reason for the negligible transmission is apparent when looking at a subcritical slope example in more detail (Fig. 4a). As depth-averaged N^2 drastically decreases up-slope of the 600-m isobath, horizontal wavelength and group velocity of the transmitted waves both decrease such that the leading wave does not reach the shelf break by $t = 10.25T$. Even at $t = 16.25T$ (not shown) the waves are almost totally dissipated (likely by multiple surface and bottom reflections) before reaching the shelf.

For a partially supercritical slope example, where $\alpha > 1$ between 520 and 680 m and $\alpha_{\max} = 1.4$ (Fig. 4b), onshore and offshore internal wave beams are apparent, originating in the upper near-critical region. The energy flux is bottom intensified where the slope is intersected by the pycnocline and is near- or supercritical. Modal decomposition of the energy flux at the base of the slope shows 9% is contained in higher modes. As with the

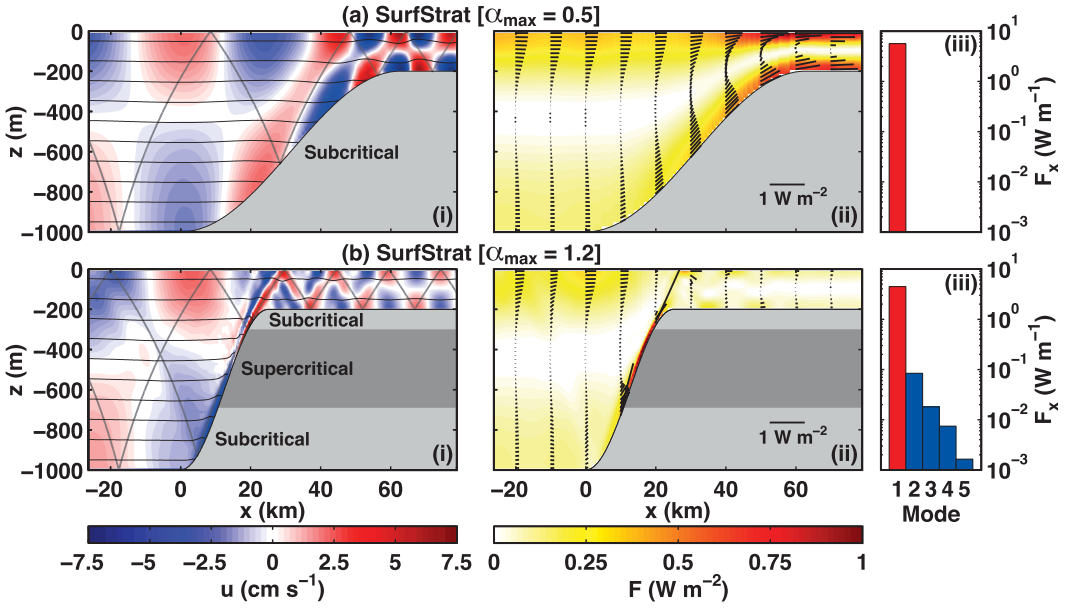

FIG. 3. Near-surface stratification examples: (a) subcritical slope, (b) partially supercritical slope. (i) Across-slope velocity (color) and vertical displacement (back lines) at $t = 10.25T$. The gray lines are M_2 internal tide characteristics. (ii) Vectors of across-slope and vertical energy flux. The underlying color is energy flux magnitude. (iii) Depth-integrated modal decomposition of across-slope energy flux at the base of the shelf slope ($x = 0$), red: onshore, blue: offshore.

partially supercritical SurfStrat example, the higher-mode energy fluxes are all offshore, consistent with scattering from the near-critical regions of the slope.

Maximum reflected energy flux is in the upper and lower layers (Fig. 5b). This may be explained by reflection of internal wave characteristics from the supercritical region of the slope, with an intermediate surface or bottom reflection. However, modal decomposition shows the majority of the reflected energy flux is in mode 1; contributions from higher modes are focused in the pycnocline. Unlike the partially supercritical SurfStrat example, the reflected energy flux does not go to zero at

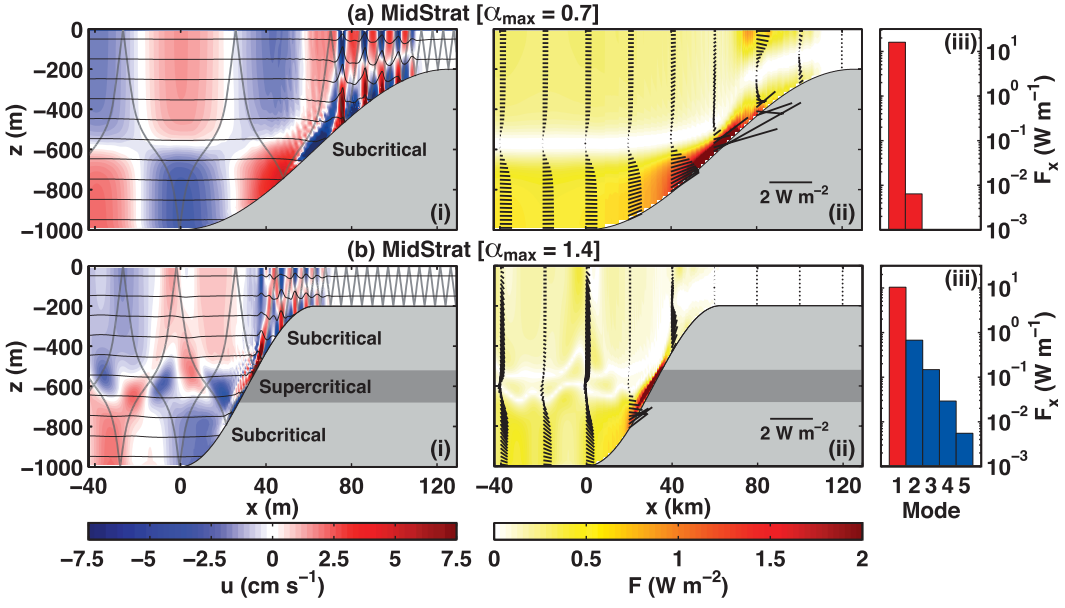

FIG. 4. As in Fig. 3, but for middepth stratification examples.

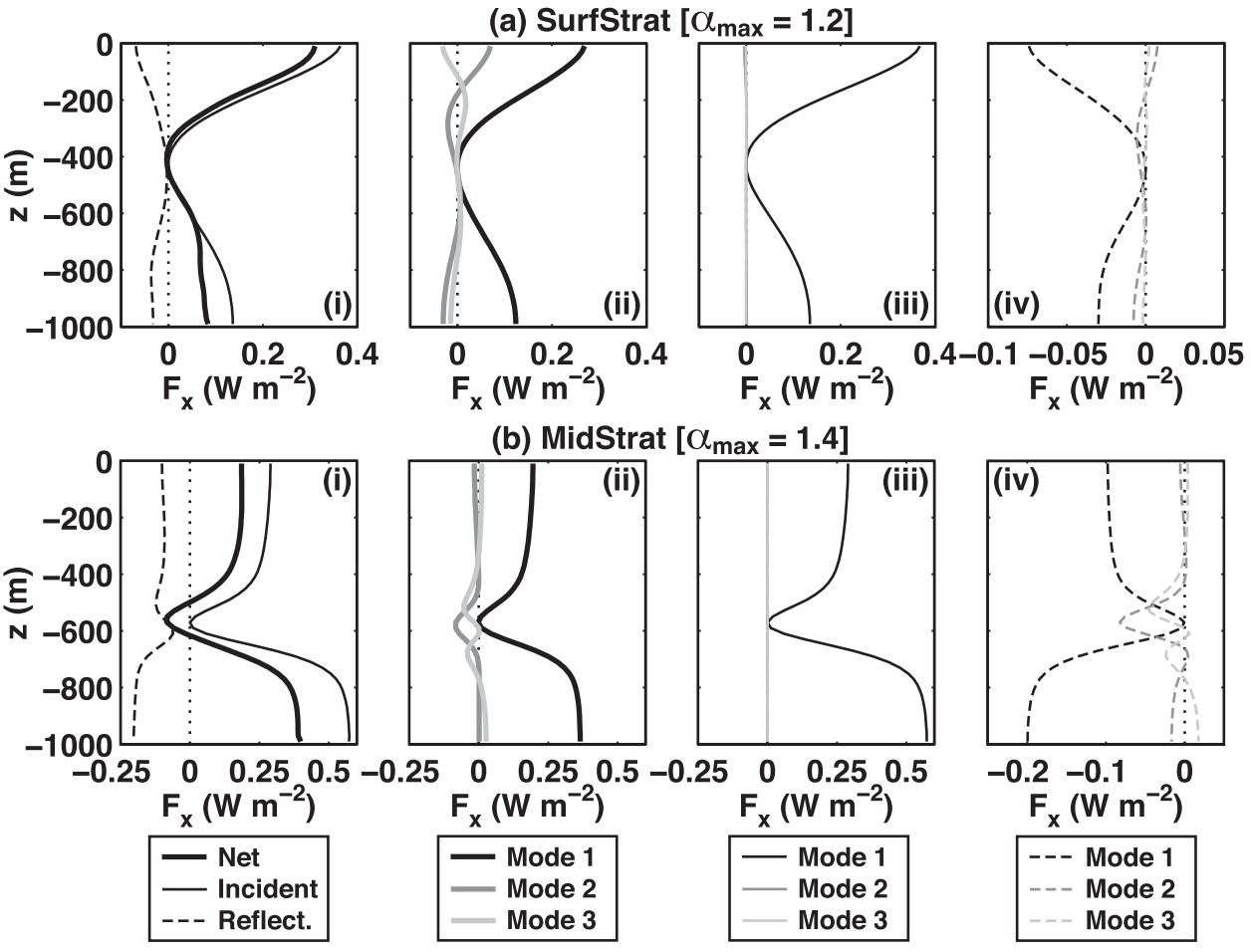

FIG. 5. (a) Near-surface stratification and (b) middepth stratification partially supercritical slope examples. (i) Net across-slope energy flux at the base of the shelf slope ($x = 0$), separated into incident (onshore propagating) and reflected (offshore propagating) components. Modal decomposition of (ii) net, (iii) incident, and (iv) reflected across-slope energy fluxes at the same location.

the mode-1 zero-crossing depth (580 m). The net energy flux is therefore offshore in the pycnocline.

This MidStrat run has stratification and topography closest to the West Shetland slope and can be used to help interpret the internal tide observations described by Hall et al. (2011). The forcing amplitude (U_0) is chosen to give a 5-m displacement amplitude, comparable to that observed on the West Shetland slope, and the depth-integrated energy flux at the 680 m isobath (the depth at the location of the observations) is 147 W m^{-1}, close to the observed 140 W m^{-1}.

From both the model and observations, maximum energy flux is located near-bottom and within the pycnocline; the observed energy flux structure is therefore consistent with a remotely generated, mode-1 internal tide. The model suggests ~40% of the incident internal tide energy flux on the West Shetland slope is reflected back offshore, the majority contained above and below the pycnocline.

d. WKB-scaling

The partially supercritical slope examples shown in Figs. 3b and 4b are WKB-scaled following Leaman and Sanford (1975) and Althaus et al. (2003) to approximate uniform stratification. The scaled depth-coordinate is $z_* = \int_z^0 N(z')/N_0\, dz'$, where N_0 is the depth-averaged buoyancy frequency off-shelf. Across-slope velocity scales as $u_* = u\sqrt{N_0/N(z)}$ and vertical displacement as $\xi_* = \xi\sqrt{N(z)/N_0}$. This scaling stretches the watercolumn where N is high and compresses the watercolumn where N is low to approximate uniform stratification (Fig. 6). Velocity is decreased (increased) where the watercolumn is stretched (compressed); vice versa for vertical displacement.

Internal wave characteristics are straight in WKB-scaled coordinates (concurrent with uniform N). However, the depth-varying stratification cases do not exactly scale to the uniform stratification case with a linear shelf

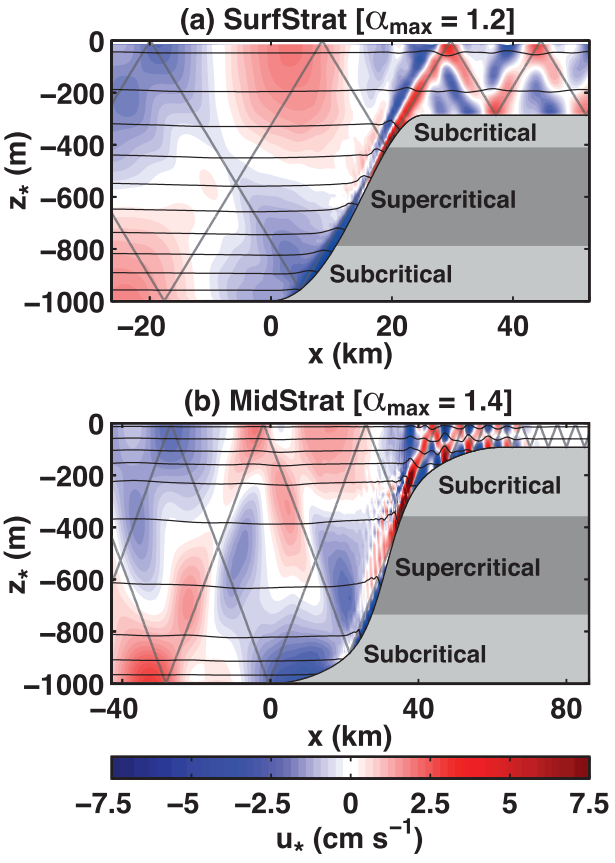

FIG. 6. (a) Near-surface stratification and (b) middepth stratification partially supercritical slope examples with WKB-scaling. Across-slope velocity (color) and vertical displacement (back lines) at $t = 10.25T$. The gray lines are M_2 internal tide characteristics.

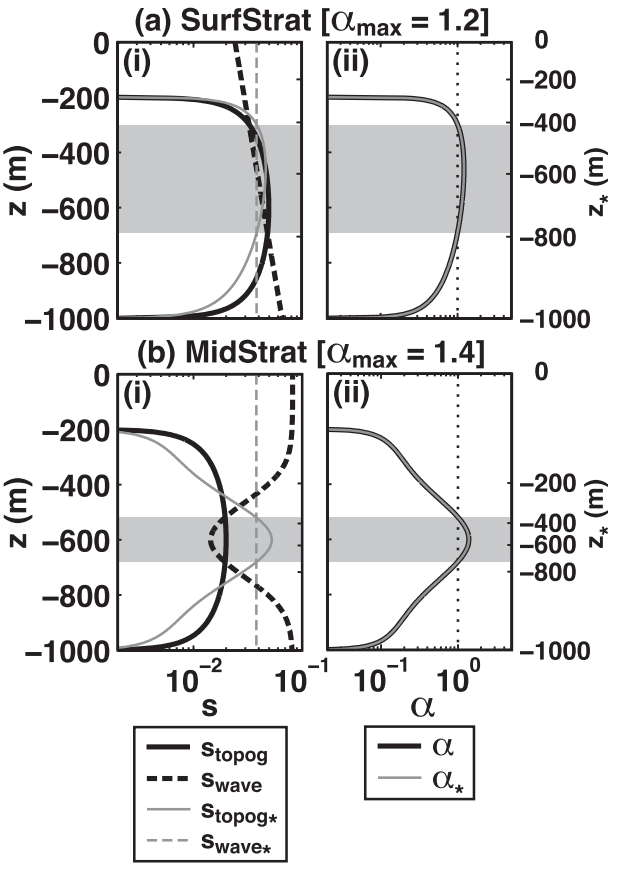

FIG. 7. Vertical projection of topographic slope (s_{topog}), internal wave characteristic slope (s_{wave}), and α for (a) near-surface stratification and (b) middepth stratification partially supercritical slope examples ($*$ denotes WKB-scaling). In (ii) the dotted line is the critical value ($\alpha = 1$). The shaded area is the depth-range the shelf slope is supercritical. The right hand axis (z_*) is the WKB-scaled depth coordinate.

slope because the scaled depth coordinate also distorts the slope topography. The term α is not altered by the scaling because s_{wave} and s_{topog} are increased (decreased) by the same factor where the watercolumn is stretched (compressed). Therefore, the partially supercritical slope examples remain both sub- and supercritical in WKB-scaled coordinates (Fig. 7), although the spatial distribution of α is altered. For the depth-varying stratification cases to exactly scale to the uniform stratification case, the slope topography has to be adjusted so that α is uniform in z-coordinates.

WKB-scaling alters the depth of the continental shelf and therefore the height of the slope. An effective slope height is calculated $h_{eff} = h_*/H_0$, where h_* is the WKB-scaled slope height; h_{eff} is 0.7 for the SurfStrat case and 0.9 for the MidStrat case (Table 1). This compares with 0.8 for the same cases without scaling and for the UniStrat case. The large effective slope height for the MidStrat case is an effect of the weak near-surface stratification and linked to the negligible internal wave transmission onto the shelf.

Although energy flux scales as $\mathbf{F}_* = \mathbf{F}N_0/N(z)$, the depth integral is not altered so the fractions of incident internal wave energy reflected and transmitted are the same. The relationships between reflection/transmission and α_{max} (Fig. 2) are therefore independent of WKB-scaling.

5. Discussion

Internal waves are an important source of energy for turbulent mixing in the ocean and may be key to maintaining the meridional overturning circulation (Munk and Wunsch 1998). The question of how much internal wave energy is reflected into the deep ocean, transmitted onto the continental shelves, and dissipated on shelf slopes has implications for large-scale circulation as well as local mixing processes.

For the set of stratification profiles and slope topographies considered here, the fraction of incident internal

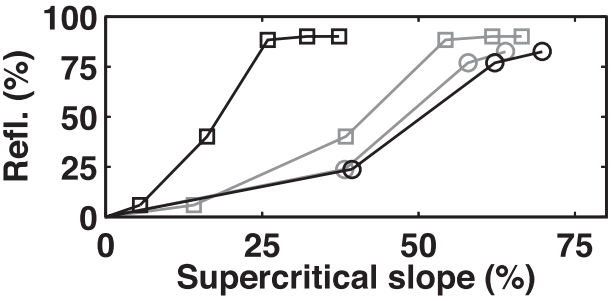

FIG. 8. Fraction of incident internal wave energy reflected back offshore for each depth-varying stratification model run, plotted against the fraction of slope height (black lines) and WKB-scaled slope height (gray lines) that is supercritical.

wave energy reflected back offshore with respect to $\alpha_{(\max)}$ falls close to the same piece-wise line (Fig. 2a). This is useful result as it allows internal wave reflection to be roughly predicted for a given buoyancy frequency profile and topographic slope. In the range $1 < \alpha_{(\max)} < 2$, the linear regression slope coefficient between decimal fraction of energy reflected and $\alpha_{(\max)}$ is $\simeq 0.8$. The fraction of energy reflected is limited by effective slope height. The maximum reflected fraction for the MidStrat case is 90%, matching the 0.9 effective slope height. For the UniStrat and SurfStrat cases the maximum reflected fraction is ~80%, concurrent with smaller effective slope heights.

It may be expected that the fraction of energy reflected should increase as the size of the supercritical region of slope increases. This is quantified as the fraction of slope height that is supercritical and increases with increasing $\alpha_{\max}$ for the curved slope topography considered here. Although there is also a relationship between the fraction of energy reflected and the supercritical fraction of slope height (Fig. 8, black lines), the results for the SurfStrat and MidStrat cases diverge. In WKB-scaled coordinates, the spatial distribution of α is altered and the size of the supercritical regions of slope can change. Using WKB-scaled topography, the supercritical fraction of slope height is increased by more than a factor of two for the MidStrat case, so there is less divergence between the results (Fig. 8, gray lines). However, $\alpha_{\max}$ is the more useful metric for predicting internal wave reflection because it is independent of WKB-scaling.

The consistent relationship between reflection and $\alpha_{\max}$ suggests that, for the depth-varying stratifications and curved slope topographies considered here, the fraction of energy reflected is dependent only on the value of $\alpha_{\max}$ and independent of the depth of the pycnocline and the depth $\alpha_{\max}$ occurs at. It also implies partially supercritical slopes reflect a similar percentage of the incident internal wave energy as entirely supercritical slopes. Dominant reflection from partially supercritical slopes increases the offshore internal wave energy flux, energy that will eventually be dissipated in the deep ocean through scattering to higher modes (Johnston and Merrifield 2003) or parametric subharmonic instability (Alford et al. 2007).

The fraction of internal wave energy transmitted onto the shelf is dependent on the depth-structure of the stratification. Unlike reflection, the fraction transmitted cannot be predicted from the value of $\alpha_{\max}$ because the depth of $\alpha_{\max}$ occurs at is also a factor. Strong near-surface stratification enhances transmission because horizontal wavelength and group velocity remain relatively large as the waves propagate up the slope (l_{eff} is large). Weak near-surface stratification inhibits transmission because horizontal wavelength and group velocity decrease rapidly (l_{eff} is small). Effective (WKB scaled) slope height is increased by weak near-surface stratification and further inhibits internal wave transmission.

Surface stratification for the MidStrat case is the same as the UniStrat case ($N^2 = 0.3 \times 10^{-5}$ s^{-2}) and both feature less transmission than the SurfStrat case (in which N^2 at the surface is an order of magnitude higher) for a given value of $\alpha_{\max}$. The negligible transmission for the MidStrat case is due to the strong middepth pycnocline that increases depth-average N^2. If near-surface buoyancy frequency is low compared to the depth-average, such as any case where the pycnocline is deeper than the continental shelf, transmitted internal waves may not reach the shelf break, even if the slope is entirely subcritical, due to decreased horizontal wavelength and group velocity up-slope of the depth of the pycnocline. This suggests dissipation of internal waves on shelf slopes, and the resulting mixing, may be enhanced at high latitudes, where low-buoyancy water masses occur near the surface.

Generation of internal wave beams only occurs on slopes that are critical, supercritical, or partially supercritical (i.e., have critical points) and the structure is dependent on the spatial distribution of α, similar to internal wave generation (Garrett and Kunze 2007). However, for all the supercritical and partially supercritical slopes considered here, the majority of the reflected energy flux is in mode 1, with only minor contributions from higher modes due to scattering from the near-critical regions of the slope. This is contrary to the results of many field observations (e.g., Nash et al. 2004) where incident low-mode internal waves are reflected back offshore to higher modes. On the Virginia continental slope, Nash et al. (2004) attributed this reflection to higher vertical wavenumbers to large areas of near-critical bathymetry ($0.7 < \alpha < 1.3$). Using the

same criterion, the near-critical area of shelf slope in SurfStrat [$\alpha_{max} = 1.2$] and MidStrat [$\alpha_{max} = 1.4$] is 60% and 18% of the slope height, respectively. As the majority of the slope in the SurfStrat example is near-critical, the reflection to low modes that dominates this run cannot simply be attributed to a small area of near-critical slope.

The dominant reflection to low-mode internal waves is likely an effect of the overly smooth, idealized slope topographies considered here. Corrugations and other small-scale topographic features are common along continental margins and increase the high-mode content of the internal wave field (Legg 2004). The absence of roughness in the model topography may go some way to explaining the relative lack of high-mode energy in these simulations. Another possibility is that the low-mode content of reflected internal waves may be underestimated in observations. In most circumstances, field measurements of internal wave energy fluxes are ''net'' values because the unmodified, incident energy fluxes are not known. It is possible that low-mode reflected energy fluxes may be underestimated due to being masked by larger-amplitude incident waves.

The results of this study may not be universal, reflection and transmission are likely to be partly dependent on the thickness and strength of the pycnocline, and the height and shape (i.e., concave or convex) of the slope. In addition, dissipation will be dependent on the bottom friction coefficient and turbulence parameterization used. Sensitivity to these parameters is beyond the scope of this study. However, the three key results presented here, 1) internal wave reflection can be independent of pycnocline depth, 2) reflected energy fluxes can be dominated by mode 1 rather than higher modes, and 3) internal wave transmission is dependent on the depth-structure of the stratification, should be considered in future investigations of internal wave reflection.

Acknowledgments. R. A. Hall was supported by a Natural Environment Research Council Ph.D. studentship, NER/S/A/2005/13812. Assistance with the setup and running of the numerical model was provided by Jiuxing Xing (National Oceanography Centre). CTD data from the California shelf slope was provided by Glenn Carter (University of Hawaii). Helpful comments on the manuscript were provided by several reviewers.

REFERENCES

Akylas, T. R., R. H. J. Grimshaw, S. R. Clarke, and A. Tabaei, 2007: Reflecting tidal wave beams and local generation of solitary waves in the ocean thermocline. *J. Fluid Mech.,* **593,** 297–313.

Alford, M. H., J. A. MacKinnon, Z. Zhao, R. Pinkel, J. Klymak, and T. Peacock, 2007: Internal waves across the Pacific. *Geophys. Res. Lett.,* **34,** L24601, doi:10.1029/2007GL031566.

Althaus, A. M., E. Kunze, and T. B. Sanford, 2003: Internal tide radiation from Mendocino Escarpmentation. *J. Phys. Oceanogr.,* **33,** 1510–1527.

Baines, P. G., 1982: On internal tide generation models. *Deep-Sea Res.,* **29,** 307–338.

Cacchione, D. A., and C. Wunsch, 1974: Experimental study of internal waves over a slope. *J. Fluid Mech.,* **66,** 223–239.

Cole, S. T., D. L. Rudnick, B. A. Hodges, and J. P. Martin, 2009: Observations of tidal internal wave beams at Kauai Channel, Hawaii. *J. Phys. Oceanogr.,* **39,** 421–436.

Dauxois, T., A. Didier, and E. Falcon, 2004: Observations of near-critical reflection of internal waves in a stably stratified fluid. *Phys. Fluids,* **16,** 1936–1941.

De Silva, I. P. D., J. Imberger, and G. N. Ivey, 1997: Localised mixing due to a breaking internal wave ray at a sloping bed. *J. Fluid Mech.,* **350,** 1–27.

Dushaw, B. D., B. D. Cornuelle, P. F. Worcester, B. M. Howe, and D. S. Luther, 1995: Barotropic and baroclinic tides in the central North Pacific Ocean determined from long-ranged reciprocal acoustic transmission. *J. Phys. Oceanogr.,* **25,** 631–647.

Eriksen, C. C., 1982: Observations of internal wave reflection off sloping bottoms. *J. Geophys. Res.,* **87,** 525–538.

Garrett, C., and E. Kunze, 2007: Internal tide generation in the deep ocean. *Annu. Rev. Fluid Mech.,* **39,** 57–87.

Gilbert, D., and C. Garrett, 1989: Implications for ocean mixing of internal wave scattering off irregular topography. *J. Phys. Oceanogr.,* **19,** 1716–1729.

Hall, R. A., J. M. Huthnance, and R. G. Williams, 2011: Internal tides, nonlinear internal wave trains, and mixing in the Faroe-Shetland Channel. *J. Geophys. Res.,* **116,** C03008, doi:10.1029/2010JC006213.

Ivey, G. N., and R. I. Nokes, 1989: Vertical mixing due to the breaking of critical internal waves on sloping boundaries. *J. Fluid Mech.,* **204,** 479–500.

Johnston, T. M. S., and M. A. Merrifield, 2003: Internal tide scattering at seamounts, ridges, and islands. *J. Geophys. Res.,* **108,** 3180, doi:10.1029/2002JC001528.

Klymak, J. M., M. H. Alford, R. Pinkel, R.-C. Lien, Y. J. Yang, and T.-Y. Tang, 2011: The breaking and scattering of the internal tide on a continental slope. *J. Phys. Oceanogr.,* **41,** 926–945.

Kunze, E., L. K. Rosenfeld, G. S. Carter, and M. C. Gregg, 2002: Internal waves in Monterey Submarine Canyon. *J. Phys. Oceanogr.,* **32,** 1890–1913.

Lamb, K. G., 2004: Nonlinear interaction among internal wave beams generated by tidal flow over supercritical topography. *Geophys. Res. Lett.,* **31,** L09313, doi:10.1029/2003GL019393.

Leaman, K. D., and T. B. Sanford, 1975: Vertical energy propagation of inertial waves: A vector spectral analysis of velocity profiles. *J. Geophys. Res.,* **80,** 1975–1978.

Legg, S., 2004: Internal tides generated on a corrugated continental slope. Part I: Cross-slope barotropic forcing. *J. Phys. Oceanogr.,* **34,** 156–173.

——, and A. Adcroft, 2003: Internal wave breaking an concave and convex continental slopes. *J. Phys. Oceanogr.,* **33,** 2224–2246.

Maas, L. R. M., 2011: Topographies lacking tidal conversion. *J. Fluid Mech.,* **684,** 5–24.

Marshall, J., A. Adcroft, C. Hill, L. Perelman, and C. Heisey, 1997: A finite-volume, incompressible Navier Stokes model for

studies of the ocean on parallel computers. *J. Geophys. Res.,* **102,** 5753–5766.

Martini, K. I., M. H. Alford, E. Kunze, S. M. Kelly, and J. D. Nash, 2011: Observations of internal tides on the Oregon continental slope. *J. Phys. Oceanogr.,* **41,** 1772–1794.

Mathur, M., and T. Peacock, 2009: Internal wave beam propagation in non-uniform stratifications. *J. Fluid Mech.,* **638,** 133–152.

Mercier, M. J., N. B. Garnier, and T. Dauxois, 2008: Reflection and diffraction of internal waves analyzed with the Hilbert transform. *Phys. Fluids,* **20,** 086601, doi:10.1063/1.2963136.

Munk, W., and C. Wunsch, 1998: Abyssal recipies II: Energetics of tidal and wind mixing. *Deep-Sea Res. I,* **45,** 1977–2010.

Nash, J. D., E. Kunze, J. M. Toole, and R. W. Schmitt, 2004: Internal tide reflection and turbulent mixing on the continental slope. *J. Phys. Oceanogr.,* **34,** 1117–1134.

——, M. H. Alford, and E. Kunze, 2005: Estimating internal wave energy fluxes in the ocean. *J. Atmos. Oceanic Technol.,* **22,** 1551–1570.

Phillips, O. M., 1977: *The Dynamics of the Upper Ocean*. 2nd ed., Cambridge University Press, 344 pp.

Slinn, D. N., and J. J. Riley, 1996: Turbulent mixing in the oceanic boundary layers caused by internal wave reflection from sloping terrain. *Dyn. Atmos. Oceans,* **24,** 51–62.

Wunsch, C., 1968: On the propagation of internal waves up a slope. *Deep-Sea Res.,* **15,** 251–258.